The Ultrastructure of Pyroxenoid Chain Silicates.
I. Variation of the Chain Configuration in Rhodonite

By D. A. Jefferson, N. J. Pugh, M. Alario-Franco,* L. G. Mallinson, G. R. Millward and
J. M. Thomas

Department of Physical Chemistry, Lensfield Road, Cambridge CB2 1EP, England

Abstract

Two samples of the silicate mineral rhondonite have been examined, in the natural state and after heat treatment, by high-resolution electron microscopy. Planar faults parallel to (001) and (110) have been observed. Computer-simulated images and optical diffraction studies have confirmed that at (001) faults strips of pyroxmangite structure are inserted into the parent rhodonite matrix. The second type of fault has been found to be equivalent to the stacking faults observed in wollastonite, and similarities and differences between this type of fault in the rhodonite and wollastonite structures are discussed.

Introduction

The pyroxenoids are a family of silicate minerals with general formula $MSiO_3$ (where M can represent Na^+, Ca^{2+}, Mg^{2+}, Mn^{2+}, Fe^{2+}, Al^{3+}) in which SiO_4 tetrahedra are corner-shared to form chains within the crystal structure. In the pyroxenoids, as opposed to the amphibole minerals, corner-sharing occurs in one direction only, such that single chains are formed, the only structural differences between the various members of the pyroxenoid family being in the repeat pattern, and hence the periodicity of the basic unit of the single $(SiO_3)_\infty$ chain.

The five known structures of minerals in the pyroxenoid group are shown schematically in Fig. 1. The simplest is the pyroxene configuration (Fig. 1*a*) where SiO_4 tetrahedra are linked in a zig-zag fashion to produce a straight chain with a 5 Å repeat unit containing two tetrahedra. The more complex structures can then be visualized as consisting of strips of the zig-zag chain, these strips being linked to one another by additional tetrahedra rotated by some 30° with respect to those of the pyroxene strip (Figs. 1*b*–1*e*).

* Present address: Facultad de Ciencias, Universidad Complutense, Madrid-3, Spain.

Where the zig-zag strips are eight tetrahedra in length, ferrosilite III (Burnham, 1966) results. Where the zig-zag strips are respectively six, four and two tetrahedra in length, pyroxmangite (Liebau, 1959), rhodonite (Lieubau, Hilmer & Lindemann, 1959), and wollastonite (Mamedov & Belov, 1956) occur. The minerals pectolite (Prewitt, 1967) and bustamite (Peacor & Buerger, 1962), which also fall within the pyroxenoid group, are believed to have the same chain configuration as that of wollastonite.

The obvious relationships between these various structures have been formalized by Liebau (1972). Although structural classification is on the basis of the configuration of the silicate chain, Liebau suggested that the octahedral ribbons, to which two corners of every SiO_4 tetrahedra are bonded, are the main factor in influencing which particular chain repeat is adopted.
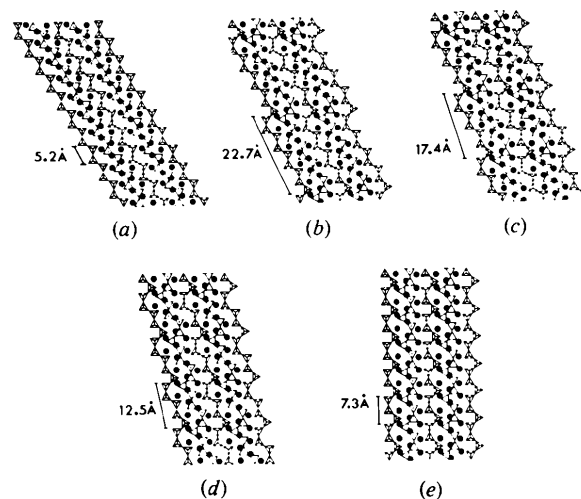

Fig. 1. Schematic projections of the five known pyroxenoid structures on to the close-packed planes. (*a*) Pyroxene, (100) projection; (*b*) ferrosilite III, (100) projection; (*c*) pyroxmangite, (100) projection; (*d*) rhodonite, (100) projection; (*e*) wollastonite, [101] projection. In each case the chain repeat distance is indicated, SiO_4 tetrahedra are shown as polyhedra, and metal cations are indicated by filled circles.

As with all silicates containing SiO_4 tetrahedra and MO_6 octahedra, a misfit will occur between those two components unless *average* dimensions of octahedral and tetrahedral cations lie within a limited range. Outside the range, any misfit can to some extent be accommodated by distortions, particularly of the $(SiO_3)_\infty$ chains, but if the misfit becomes large a change in structural configuration will be required since incommensurate sublattices are unlikely in view of the requirements of electroneutrality. Liebau envisaged the pyroxenoids as an example of this behaviour, with progressively more frequent breaking of the basic, zig-zag pyroxene chain, and consequent insertions of extra tetrahedra, as the size of the octahedral cation becomes greater. This cumulates in the wollastonite structure (Fig. 1e), where only pairs of the original zig-zag chain remain, and any further increase in octahedral cation size necessitates an abandonment of the chain configuration and the adoption of ring structures. More recently, Ohashi & Finger (1975) have suggested that pressure and temperature of formation have a similar effect to variation in cation size.

If the pyroxenoids are truly a complete structural series it might be expected that, under certain conditions of temperature, pressure and composition, a situation could arise where more than one chain configuration would be stable and intergrowths could occur. Temperature-induced topotactical changes in structure have been observed by single-crystal X-ray methods, for rhodonite/wollastonite (Dent-Glasser & Glasser, 1961) and pyroxmangite/rhodonite (Maresch & Mottana, 1976; Aikawa, 1979) but studies of this type give little indication of the relative sizes and distribution of domains of one structure type within another. These latter factors are important because there should, in principle, be at least one structural configuration, either one of those already known, or one hitherto unreported, for any conditions of formation and composition, in an analogous manner to the behaviour of certain metal oxides (Wadsley, 1964). Accordingly, an electron microscopic investigation of the mineral rhodonite was undertaken, as this technique alone could give unambiguous information on the disposition and number of structural irregularities.

Experimental

Two samples of rhodonite were selected, one from Devon, England and one from Pajsberg, Varmland, Sweden. The latter (BM No. 50045) was supplied by Dr A. C. Bishop of the British Museum. Samples were examined in the natural state and after several hours of heat treatment at 1070 K in a vacuum furnace. Specimens of crushed grains were deposited from suspension onto copper grids which had been pre-coated with holey carbon films, and were examined in a Siemens Elmiskop 102 electron microscope equipped with a double-tilt ($\pm45°$) goniometer stage. Micrographs were recorded at magnifications in the range $250\,000$–$500\,000 \times$.

In any attempt to characterize structural imperfections observed in micrographs of relatively close-packed structures, care is necessary in interpretation of image contrast and, in particular, the true *structural* resolution of the instrument concerned (Thomas & Jefferson, 1978) must be taken into account. For the Siemens 102, operating under optimum conditions, this figure of resolution is of the order of $3\cdot8$ Å, greater than cation–cation distances in rhodonite, which range from $2\cdot5$ to $3\cdot5$ Å. For this reason the images obtained could not be regarded as a complete representation of the crystal structure, being merely the superposition of various fringe systems showing some, but not all, of the features associated with the crystal itself.

To some extent, the resolution problem can be overcome by employing instruments with greater structural resolution (*ca* 2 Å) and this has proved practicable with pyroxenoids (Jefferson, Thomas, Mallinson & Smith, 1979) but conditions for good correspondence between image contrast and object structure are more severe at the higher resolution. Furthermore, even at 2 Å resolution, interpretation of image contrast in terms of cation positions and silicate chain configuration is possible only in one structural projection: consequently, for a preliminary study such as this, lower resolution examination was preferred.

In order to extract reliable information from images obtained at *ca* 4 Å resolution, it was necessary to predict by computer simulation the images obtained from perfect rhodonite and a series of models of defective rhodonites over a range of values of crystal thickness and objective-lens defocus, from the known aberration constants of the Siemens 102. This was achieved with programs written by one of us (DAJ) which employed the multislice method of Cowley & Moodie (1957), models for defective structures being calculated with artifically large unit cells in the manner of Grinton & Cowley (1971). Although simulated images of the latter type in general contained erroneous contrast arising from overlapping Fourier images (Rogers, 1969), this effect was relatively slight over a useful range of objective-lens defocus and crystal thickness, within which an excellent agreement with experimental images was obtained. When comparison with experiment indicated that an important factor determining the nature of image contrast was objective-lens defocus, an attempt was also made to simulate this effect upon models of defects by optical reconstruction which could not simulate the effect of increasing specimen thickness, but enabled much larger arrays of atoms to be employed. This technique also gave some measure of agreement with observed images.

Results

(001) *planar defects*

Defects exhibiting a variation in periodicity parallel to the main direction, and hence suggesting a local alteration in chain configuration, were observed in both natural and heated rhodonites, more numerous in the latter, but relatively infrequent in all cases. Fig. 2(*a*) shows one such defect, viewed at the crystal edge with the electron beam parallel to [100]. The apparent periodicity of the defect is some 5 Å, in the chain direction, compared to 12·5 Å for the rhodonite matrix.

Fig. 2(*b*) shows the same defect, in a slightly thicker region of the crystal, where the periodicity indicated is 17·5 Å, closely corresponding to the pyroxmangite repeat. The plane of the defect is (001) and in both cases an offset of (02̄1) fringes can be noted as they intersect the defect. This offset was measured as approximately 0·4 of the (02̄1) fringe spacing. (010) fringes were less clearly defined, but also showed a significant offset at the defect, as illustrated in Fig. 2(*b*).

All defects observed in [100] projection showed identical behaviour to that illustrated in Fig. 2, but different phenomena were noted in other projections. Fig. 3 illustrates a similar feature, again parallel to
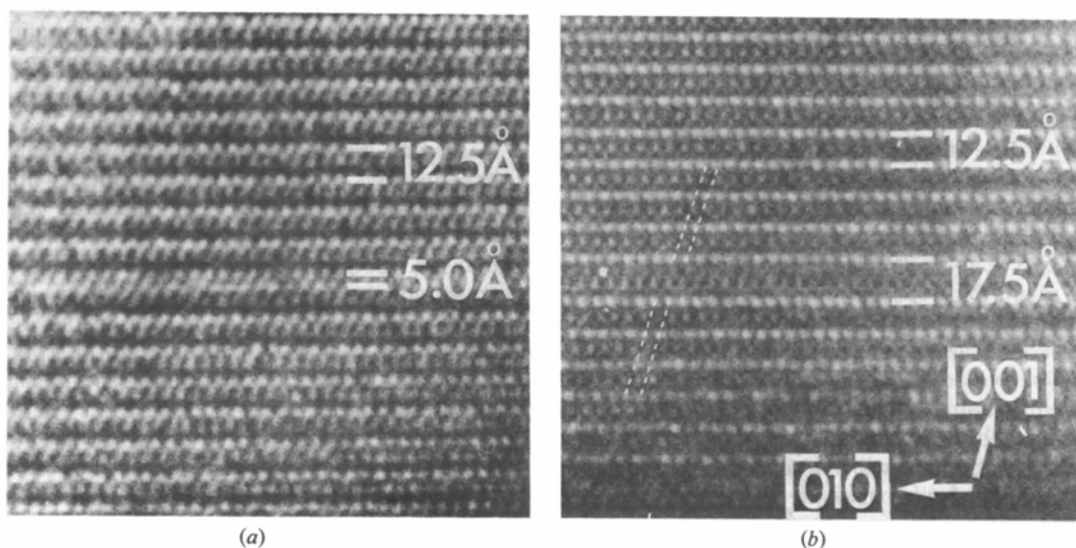

Fig. 2. Electron micrograph of a pyroxmangite-like defect in rhodonite (*a*) at the crystal edge and (*b*) in a thicker region of the crystal. In each case the electron beam is parallel to [100], and the *apparent* periodicity of the defect is indicated. In (*b*) the offset of (010) fringes on crossing the defect is also shown.
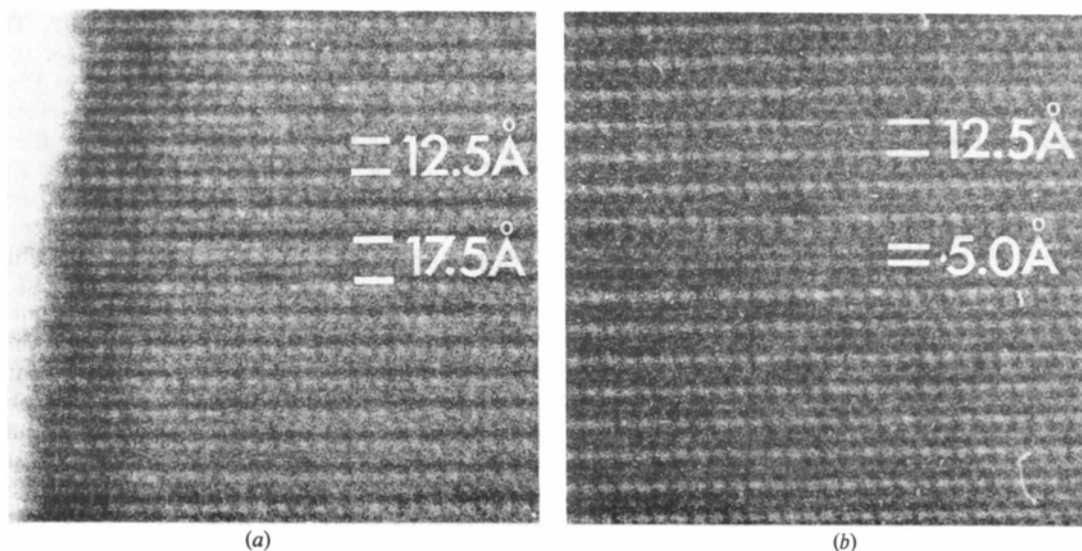

Fig. 3. Electron micrograph of a pyroxmangite-like defect taken with the electron beam parallel to [1 1̄ 0] (*a*) at the crystal edge and (*b*) at a slightly thicker region, and at a different defocus. Again the apparent periodicity is indicated.

(001), observed in [1Ī0] projection. Again, an apparent alteration in the periodicity at the defect was noted, this being 17·5 Å visible at the crystal edge (Fig. 3a), altering to a faint 5 Å repeat in thicker regions (Fig. 3b). In thicker parts of the crystal the observed periodicity was found to be markedly dependent on objective-lens defocus and, in this projection, no marked offset of fringes was noted as they intersected the defect. In all cases where defects parallel to (001) were noted, they were found to extend completely throughout the crystal concerned, with no observable strain contrast, and no side-stepping along their length.

(110) *planar defects*

A second type of imperfection was also observed in rhodonite samples, a typical example being illustrated in Fig. 4(a). Defects of this second type were observed with the electron beam parallel to [1Ī0], and were parallel to (110) planes. In contrast with (001) defects, (110) imperfections were of finite length (ca 1000–2000 Å) and although fringes intersecting the plane of the defect were offset, the magnitude of the offset varied from zero to 0·5 along the length of the defect, as shown in the defect AB of Fig. 4(a). Most of the defects

of this type were parallel to a crystal edge and found only in thinner regions, typified by defect CD in Fig. 4(a): occasionally they could be found almost perpendicular to the edge, as illustrated in Fig. 4(b). In many cases the (110) defects would appear to terminate within the crystal and then reappear further away, usually on a different (110) plane. Invariably, the gap between the two observed defect regions would be characterized by strain contrast, similar to that observed around dislocations. One such example is the defect pair AB and CD in Fig. 5(a). More complex behaviour was also observed, as shown in Fig. 5(b). In this latter case defect AB appears to re-emerge at CD, and is also associated with a second emergent defect EF. Once again, strain contrast is evident between the latter two features.

Discussion

The alteration in lattice periodicity at (001) planar defects is quite distinctive and abrupt, which would not be expected if the defect occurred only along a line within the crystal, or along a plane inclined at some angle to (001) planes. It would therefore seem
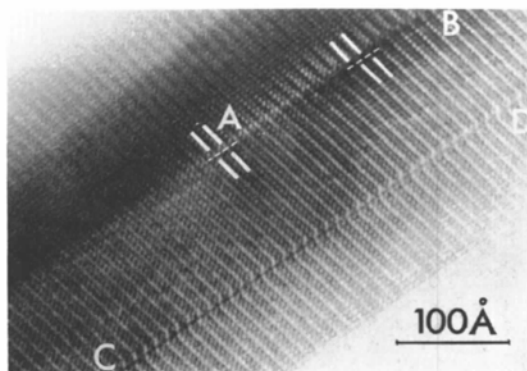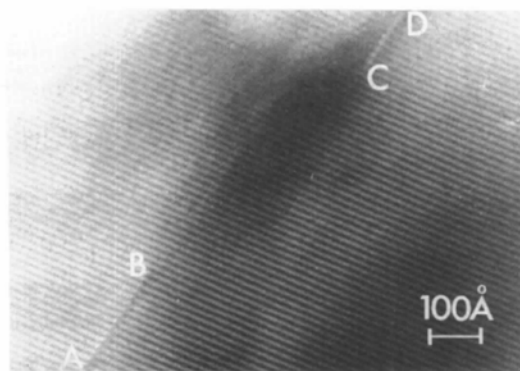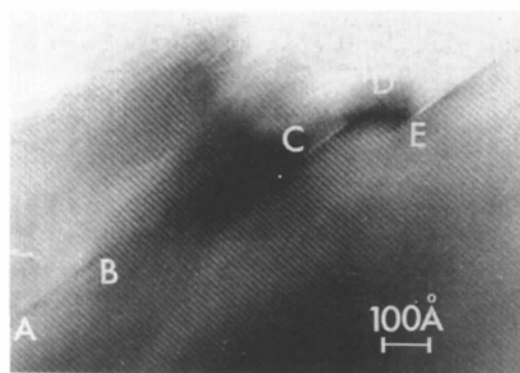

(a)
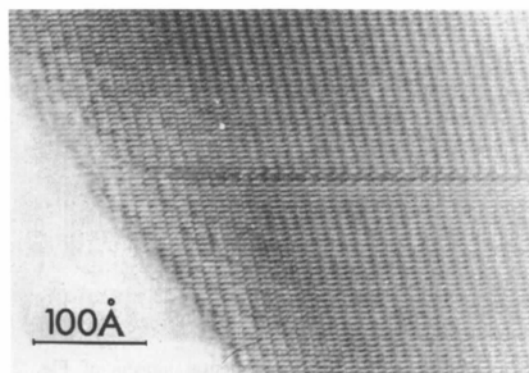
(b)

Fig. 4. (a) and (b) Stacking faults in rhodonite, viewed with the electron beam parallel to [1Ī0]. In (a), two defects are present, AB and CD, the variation in offset at the former being indicated.

(a)

(b)

Fig. 5. (a) and (b) Stacking faults in rhodonite which vanish and reappear on a different plane. In both cases considerable strain contrast is evident.

reasonable to assume that the defects are genuinely planar ones, parallel to (001), and that defects observed in both [100] and [1$\bar{1}$0] axis projections are identical types of imperfection. Owing to the resolution limit discussed previously, it is impossible to determine directly the nature of such defects from the observed image contrast, but the observed increase in periodicity to 17·5 Å as opposed to the 12·5 Å of the normal rhodonite suggests that a strip of the pyroxmangite structure has been inserted into the rhodonite matrix, and the circumstantial evidence to support this hypothesis is strong. For example, in [100]-axis projection, the calculated offset of (0$\bar{2}$1) fringes crossing a unit-cell-wide strip of pyroxmangite within rhodonite is 0·39, comparing favourably with the experimentally measured value of 0·4, and in [1$\bar{1}$0] projection, a very slight offset of fringes is predicted at such a defect, as observed. Furthermore, the manner in which defects of the (001) type extend laterally throughout the crystal can readily be envisaged if the model is assumed for such defects. From Figs. 1(c) and 1(d) it is evident that if, at any point in the crystal, a seven-tetrahedron repeat is inserted instead of the normal five, this will cause changes in the underlying octahedral ribbon, which in turn will necessitate a seven-tetrahedron repeat in an adjacent chain, and so on right across the

crystal, any termination of this process requiring a much more drastic structural rearrangement.

Nevertheless, evidence such as this is circumstantial, and a unit-cell-wide strip of wollastonite, although it might not be expected to produce the observed alterations in periodicity, would give similar fringe offsets in [100] and [1$\bar{1}$0] projections, although in an opposite sense. More complicated insertions could also be envisaged. In order to assign a unique structure to defects of this type, a computer-simulated image was calculated for a unit cell containing one repeat unit of pyroxmangite flanked by a pair of rhodonite repeat units. Results for this 405-beam calculation, in [100] projection, together with the structural model used, are shown in Fig. 6. Any of the computer-simulated images illustrated therein show the poor correspondence between image contrast and the detailed atomic structure either at the defect or in the normal rhodonite lattice. However, the variation in the *apparent* periodicity at the defect with increasing crystal thickness (Z) is clearly simulated, in agreement with observed images. Near the so-called Scherzer focus of *ca* 950 Å for the instrument used (Erikson & Klug, 1971), the apparent periodicity of the defect is some 5 Å for crystals of up to 100 Å thickness, but becomes a 17·5 Å periodicity by the time the crystal thickness has increased to 300 Å. In Fig. 6, computed images are
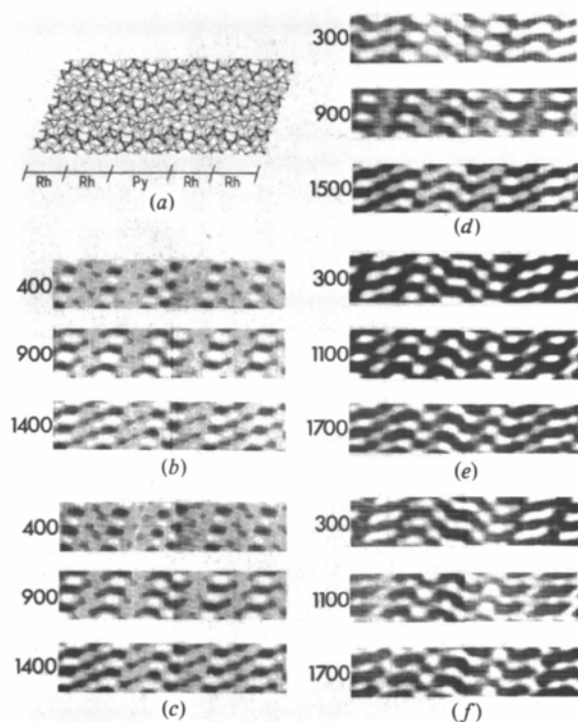

Fig. 6. Structural model and [100] computer-simulated images for a pyroxmangite-like defect in rhodonite. (a) Structural model. Computed image for (b) $Z = 25$ Å, (c) $Z = 50$ Å, (d) $Z = 100$ Å, (e) $Z = 200$ Å, (f) $Z = 300$ Å. Simulated objective-lens defocus is indicated alongside each image.
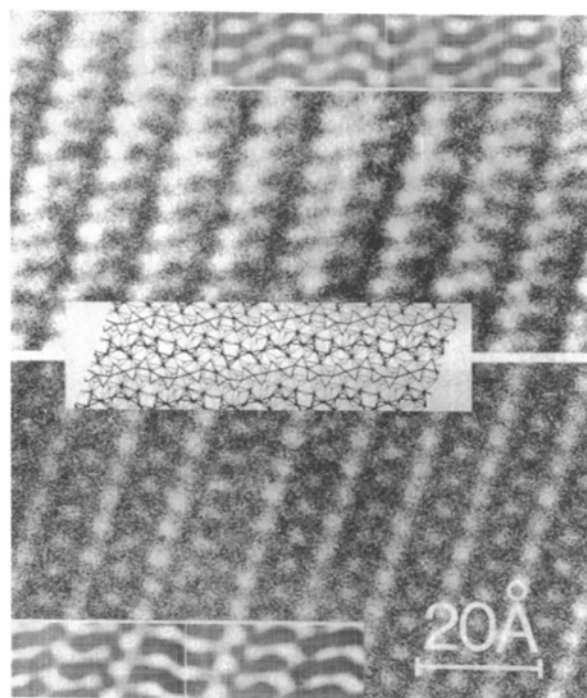

Fig. 7. Comparison of the experimental images of Fig. 2 with computed ones. The upper image is matched at $Z = 50$ Å, defocus of 1000 Å, the lower image corresponds to a thickness of 300 Å and a defocus of 1600 Å. The structural model used is also shown.

illustrated at positions of objective-lens defocus producing maximum fringe contrast. For a thickness of 200 Å, it is difficult to decide whether the apparent periodicity indicated is 5 or 17·5 Å, although at the values of defocus used for the images shown, the former appears to predominate. When the simulated images are compared with the experimental ones of Fig. 2 (Fig. 7), the manner in which this behaviour is shown by the defects observed is clearly predicted. There would therefore appear to be little doubt that the observed defects were of strips of pyroxmangite-like structure in rhodonite. A naive interpretation of the observed behaviour of the image with increasing crystal thickness is that, in the thinner regions, the image contrast highlights the 5 Å spacing of the pair of tetrahedra which must be inserted into the rhodonite repeat to produce pyroxmangite. For greater thicknesses, however, the true structural repeat of the defect becomes apparent.

Computer simulation of defect images in complex structures is time-consuming and suffers from the disadvantage of an artificially imposed large periodicity discussed previously. Accordingly, an attempt was made to see if some of the features of defect images could be simulated by optical diffractometry with masks made from idealized models of both pyroxmangite-like and wollastonite-like defects in rhodonite. The results for [100] projection of both models are shown in Fig. 8. For both models, an aperture was placed in the diffraction plane to limit the number of beams contributing to the final image, as shown, and the reconstructed image was recorded at various values of defocus of the recombining lens when maximum contrast was observed. In this simulation the pyroxmangite-like defect (Fig. 8a) showed both 17·5 and 5 Å periodicities with variation of defocus, whereas the wollastonite-like model showed only a 7·5 Å repeat at the defect indicating that, in principle, the two types of defect could be distinguished in this way. Owing, however, to the experimentally observed fact that the change of apparent periodicity of the pyroxmangite-like defect occurred principally with increasing thickness, it would appear that optical diffraction techniques, which cannot simulate the latter effect, are at best a poor substitute for multislice image calculations, in spite of the increasing complexity of the calculations for defect structures.

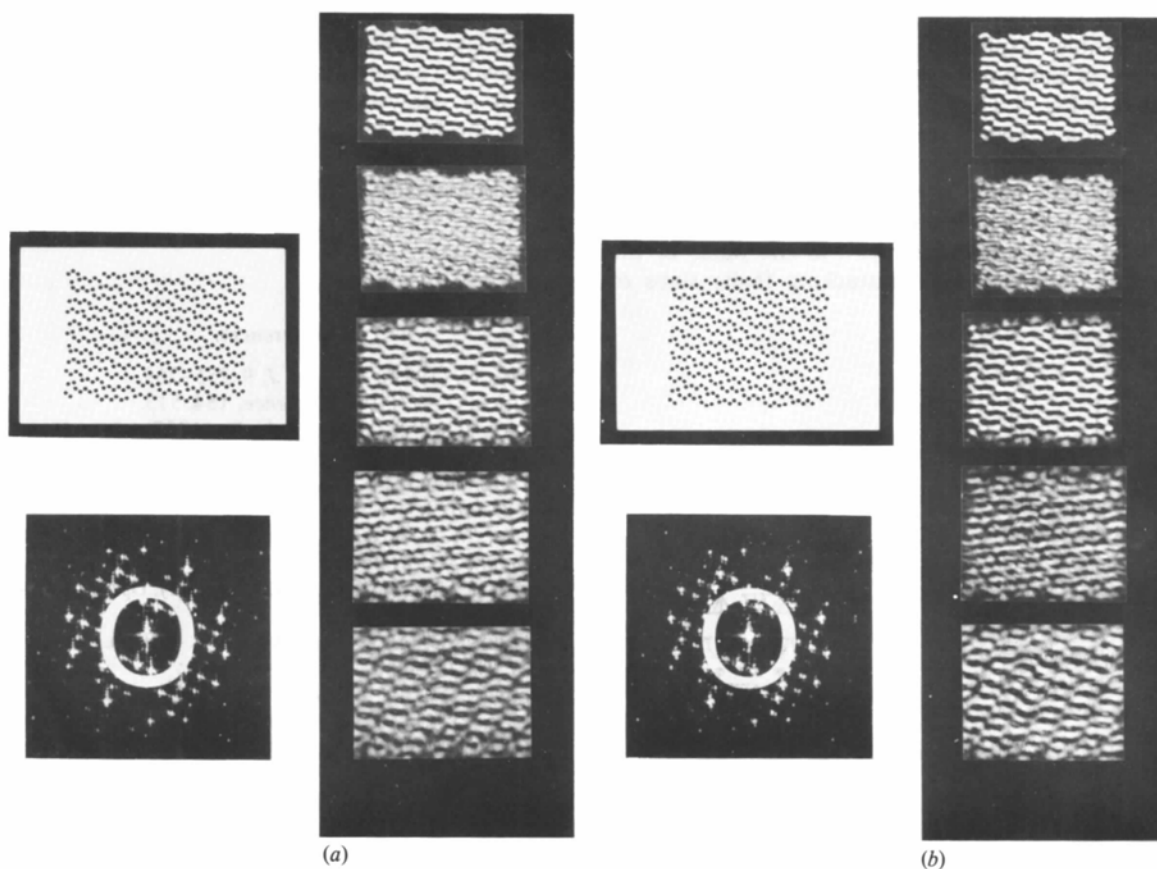(110)-type defects constituted a more difficult case to

Fig. 8. Optical diffractometer simulations of defects in rhodonite. (a) Pyroxmangite-like defect; (b) wollastonite-like defect. In each case a negative of the mask used, the optical diffraction pattern and the recombined image at five positions of maximum contrast are shown.

analyse. As with the (001) defects, the sharp image contrast at the line of the defect, coupled with the fact that (110) defects were only observed in projection down [1$\bar{1}$0], suggested that the latter were true planar defects on (110). However, the fact that (110)-type defects were of limited extent in two dimensions made image calculations of proposed models for these defects virtually impossible, owing to the extremely large number of beams which would have to be handled. Consequently their exact nature could only be inferred by analogy with similar defects observed in wollastonite. Planar stacking faults have frequently been observed in wollastonite (Jefferson & Thomas, 1975) and play a role in the determination of the polytypism of this mineral. The plane of these defects in wollastonite is (100), which is equivalent, owing to a change in axes, to (110) in rhodonite. It therefore seems likely that the (110)-type defects in rhodonite are similar to those observed in wollastonite, bearing in mind the close similarity of the two structures. Nevertheless, whereas such defects are common in wollastonite, they occur only rarely in rhodonite, and invariably are of limited extent, a feature only occasionally found in wollastonite (Morales, Jefferson, Hutchinson & Thomas, 1977). Also, although regular arrays of defects in wollastonite can produce alternative polytypes, no polytypism has been noted in rhodonite.

A possible explanation for the differences in behaviour of this type of defect in the two structures is indicated in Fig. 9. Here the structure of wollastonite is projected in a direction approximately perpendicular to the plane of the octahedral ribbons (Fig. 9a), and are also shown schematically viewed down the chain axis (Fig. 9b). In wollastonite the plane of the stacking faults is inclined at approximately 45° to the plane of the octahedral ribbons. At such stacking faults slabs of structure are displaced in the direction of the chain, as shown in Fig. 9(a), a process which, judging from the frequency with which such faults occur, involves little, if any, strain energy. When the rhodonite structure is viewed along the chain axis, similar defects appear equally likely, but when this structure is viewed in the plane of the octahedral ribbons, as in Fig. 1(d), one important difference between the two structures is evident, namely that, whereas in wollastonite the octahedral ribbon is straight, the equivalent structural component in rhodonite is kinked, and adjacent ribbons are locked togther. Any displacement of one ribbon with respect to its predecessor in rhodonite must therefore necessitate considerable structural disruption, particularly to the silicate chain which bridges the gap between ribbons, and if such defects occur, they might well be expected to have high stacking-fault energy and consequently be of limited extent. As this corresponded exactly to the behaviour observed in images of (110)-type defects in rhodonite, it was concluded that these were wollastonite-like stacking faults, of limited lateral extent bounded by a dislocation loop. This agrees with the observed images of Fig. 5, the strain contrast being associated with the dislocation loop.

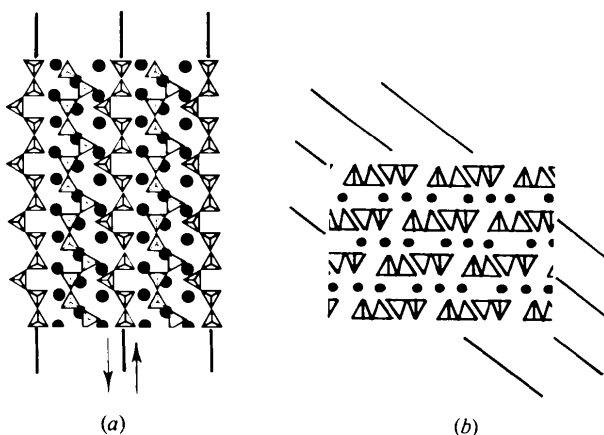Fig. 9. Geometry of stacking faults in wollastonite: (a) |101| projection; (b) |010| projection. Directions of mutual displacement are indicated in (a).

References

AIKAWA, N. (1979). Mineral. J. 9, 255–269.
BURNHAM, C. W. (1966). Science, 154, 513.
COWLEY, J. M. & MOODIE, A. F. (1957). Acta Cryst. 10, 609–619.
DENT-GLASSER, L. S. & GLASSER, F. P. (1961). Acta Cryst. 14, 818–822,
ERIKSON, M. P. & KLUG, A. (1971). Philos. Trans. R. Soc. London, Ser. B, 261, 105–118.
GRINTON, G. R. & COWLEY, J. M. (1971). Optik (Stuttgart), 34, 221–233.
JEFFERSON, D. A. & THOMAS, J. M. (1975). Mater. Res. Bull. 10, 761–768.
JEFFERSON, D. A., THOMAS, J. M., MALLINSON, L. G. & SMITH, D. J. (1979). Electron Microscopy and Analysis 79, edited by T. MULVEY, pp. 102–104. London: Institute of Physics.
LIEBAU, F. (1959). Acta Cryst. 12, 177–181.
LIEBAU, F. (1972). Handbook of Geochemistry, Vol. II, chap. 14. Berlin: Springer-Verlag.
LIEBAU, F., HILMER, W. & LINDEMANN, G. (1959). Acta Cryst. 12, 182–187.

MAMEDOV, KH. S. & BELOV, N. V. (1956). *Dokl. Akad. Nauk SSSR*, **107**, 463–466.

MORALES, J., JEFFERSON, D. A., HUTCHINSON, J. L. & THOMAS, J. M. (1977). *J. Chem. Soc. Dalton Trans.* pp. 1834–1836.

MARESCH, W. V. & MOTTANA, A. (1976). *Contrib. Mineral. Petrol.* **55**, 69–79.

OHASHI, Y. & FINGER, L. W. (1975). *Ann. Rep. Carnegie Inst. Washington*, **74**, 564–569.

PEACOR, D. R. & BUERGER, M. J. (1962). *Z. Kristallogr.* **117**, 331–343.

PREWITT, C. T. (1967). *Z. Kristallogr.* **125**, 298–316.

ROGERS, G. L. (1969). *J. Microsc. (Oxford)*, **89**, 121–124.

THOMAS, J. M. & JEFFERSON, D. A. (1978). *Endeavour*, **2**, 127–136.

WADSLEY, A. D. (1964). *Non-Stoichiometric Compounds*, Ch. 3, edited by L. MANDELCOM. London: Academic Press.

Effects of Phase Errors on E Maps

BY A. M. SILVA* AND D. VITERBO†

Department of Physics, University of York, Heslington, York YO1 5DD, England

Abstract

A systematic investigation of the effect of phase errors of different types on E maps is presented. Both random and systematic errors have been considered with distributions depending in different ways on the resolution of the data. Considerably large random errors can be tolerated without great loss of structural information in the E maps, while smaller systematic errors have greater destructive effects. These effects are explained by the introduction and analysis of a phase-error function.

Introduction

The final outcome of any direct-methods procedure is a set of approximate phases with which an E map is computed. It is obvious that the quality of the map is related to the errors in the phases and it is this relationship which we study in this work. The interest of this analysis is also related to the possibility of comparing the power of different direct-methods procedures, from tests on known structures, by giving the value of the mean phase error or the root-mean-square deviation of the phases.

Phase errors and resolution

Parthasarathy (1978), assuming a normal distribution for the errors of the atomic positions, has calculated the

---

average of the absolute value of the phase errors, $\langle |\Delta\varphi| \rangle$, as a function of the average of the absolute value of the coordinate errors, $\langle |\Delta r| \rangle$, for different resolutions. An analysis of Fig. 1‡ shows that, at a given value of $\langle |\Delta r| \rangle$, the phase error is high at high resolution and low at low resolution. For instance, we can see that for $\langle |\Delta r| \rangle = 0.4$ Å the corresponding phase error is 70° at a resolution of 0.77 Å, while it is 13° at $R = 5$ Å.

From Fig. 1 we have graphically derived Fig. 2 which within the error of the graphical derivation shows a linear trend of $\langle |\Delta r| \rangle$ as a function of the resolution for different values of $\langle |\Delta\varphi| \rangle$. The extrapolation of these lines to $R = 0$ indicates that, when assuming a normal distribution for Δr, with an infinite set of data the structure is exactly defined even when the average phase error is very close to 90° ($\langle |\Delta\varphi| \rangle = 90°$ corresponds to completely random phases).

From these observations we can infer that it is more important to consider not only the overall average phase error but also the distribution of the error as a function of the resolution. In fact, as far as the consequences on the accuracy of the atomic positions is concerned, a set of phases with relatively high overall $\langle |\Delta\varphi| \rangle$, due to large errors in the high-angle reflexions, will be preferable to the same set of reflexions with smaller $\langle |\Delta\varphi| \rangle$ but with large errors in the low-angle reflexions.

In order to verify this hypothesis we have performed some tests on the known structure of a photolysis product (Karle, Karle & Estlin, 1967) (KARLE: $P2_1 2_1 2_1$, 17 atoms in the asymmetric unit). Using a routine which generates random numbers with a normal

---

‡ Fig. 1 is a reproduction of Fig. 3(*a*) of the paper by Parthasarathy (1978) with a modified notation.